ACS MEASUREMENT SCIENCE Au
AN OPEN ACCESS JOURNAL OF THE AMERICAN CHEMICAL SOCIETY

pubs.acs.org/measureau

Article

Evaluating the Utility of Temporal Compression in High-Resolution Traveling Wave-Based Cyclic Ion Mobility Separations

David L. Williamson and Gabe Nagy*

Cite This: *ACS Meas. Sci. Au* 2022, 2, 361−369

Read Online

ACCESS | Metrics & More | Article Recommendations | Supporting Information

ABSTRACT: Ion mobility spectrometry coupled to mass spectrometry (IMS-MS) is slowly becoming a more integral part in omics-based workflows. With the recent technological advancements in IMS-MS instrumentation, particularly those involving traveling wave-based separations, ultralong pathlengths have become readily available in commercial platforms (e.g., Select Series Cyclic IMS from Waters Corporation and MOBIE from MOBILion). However, a tradeoff exists in such ultralong pathlength separations: increasing peak-to-peak resolution at the cost of lower signal intensities and thus poorer sensitivity of measurements. Herein, we explore the utility of temporal compression, where ions are compressed in the time domain, following high-resolution cyclic ion mobility spectrometry-mass spectrometry-based separations on a commercially available, unmodified platform. We assessed temporal compression in the context of various separations including those of reverse sequence peptide isomers, chiral noncovalent complexes, and isotopologues. From our results, we demonstrated that temporal compression improves IMS peak intensities by up to a factor of 4 while only losing ∼5 to 10% of peak-to-peak resolution. Additionally, the improvement in peak quality and signal-to-noise ratio was evident when comparing IMS-MS separations with and without a temporal compression step performed. Temporal compression can readily be implemented in existing traveling wave-based IMS-MS platforms, and our initial proof-of-concept demonstration shows its promise as a tool for improving peak shapes and peak intensities without sacrificing losses in resolution.

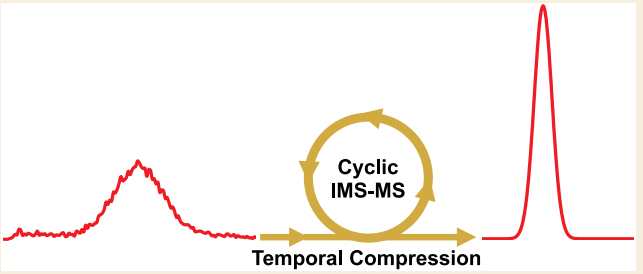

KEYWORDS: *ion mobility spectrometry, mass spectrometry, enantiomers, temporal compression, instrumentation, method development, separation science*

INTRODUCTION

Ion mobility spectrometry-mass spectrometry (IMS-MS) is an analytical method where ions are separated in the gas phase, under the presence of an electric field, based on their mobilities (i.e., size, shape, and charge).[1−3] IMS-MS has gained traction in existing analytical workflows for aiding in structural elucidation, isomer/isobar separation, and data deconvolution, among others.[4−7] Much of this recent progress has been enabled by continued improvements in instrumentation and other technological advances. While each of the many available IMS-MS modalities, such as trapped ion mobility spectrometry (TIMS),[8] drift tube ion mobility spectrometry (DTIMS),[9] field asymmetric ion mobility spectrometry (FAIMS),[10] and traveling wave ion mobility spectrometry (TWIMS),[3] offers their own unique advantages in helping solve complex problems in chemical systems, one of the most recent technological advancements in IMS is the development of extended pathlengths in traveling wave-based IMS-MS separations.[11−13]

Since IMS resolution scales approximately by the square root of the separation pathlength (e.g., a 100 m separation would provide 10 times higher resolution than a 1 m separation), longer IMS separations are very attractive for resolving very structurally similar molecules, such as cis/trans lipid isomers, peptide epimers, oligosaccharide anomers, and isotopologues/isotopomers.[12,14−19] These longer pathlength implementations are made possible by the lower voltage requirements in TWIMS and not possible in other IMS modalities, such as the large voltage drop required in DTIMS to achieve even a few meters of separation.[1−3] Currently, two commercially available traveling wave-based IMS-MS platforms (structures for lossless ion manipulations, MOBIE, from MOBILion, and the Select Series Cyclic IMS, cIMS, from Waters Corporation) have exploited this and achieved separation pathlengths >10 m and up to 2 km in a homebuilt platform.[12,15] Both SLIM IMS-MS and cIMS-MS utilize traveling wave separations, giving added flexibility and

Received: March 11, 2022
Revised: May 25, 2022
Accepted: May 26, 2022
Published: June 7, 2022

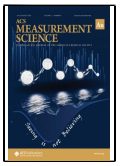

https://doi.org/10.1021/acsmeasuresciau.2c00016
ACS Meas. Sci. Au 2022, 2, 361−369

customization for experiments (e.g., IMS/IMS, peak selection, etc.).

In IMS-MS, two benchmarks are often used to describe a given separation: resolution and sensitivity.[20,21] IMS resolution between two species ("a" and "b") can be defined by eq 1, where t_a and t_b are their arrival time species with peak widths at half-maximum (FWHM). Sensitivity in IMS-MS can often be considered in terms of the signal to noise in both the IMS (i.e., peak quality) and MS (i.e., m/z of interest) dimensions. In IMS, peak widths are a result of contributions from both gate width (e.g., injection pulse from an ion funnel), peak broadening from diffusion,[22,23] and other factors such as Coulomb repulsion and post-separation dispersion.[24,25] In SLIM IMS or cIMS, resolution of very structurally similar species has been shown largely due to the ultralong separation pathlengths that are possible.[16−18,26−28] However, at these extremely long pathlengths, sensitivity will suffer due to diffusion, especially when ion injection is performed with an ion funnel. From this, it becomes evident that there exists a compromise between sensitivity and resolution in ultralong pathlength IMS-MS-based separations. For example, at shorter pathlengths, increased sensitivity is possible with limited IMS resolution, while at longer pathlengths, IMS resolution will increase at the cost of sensitivity.

$$R_{pp} = 1.18\left(\frac{t_b - t_a}{\mathrm{FWHM}_a + \mathrm{FWHM}_b}\right) \quad (1)$$

Thus, one of the ultimate goals of IMS-MS technology is to develop a method that can maintain IMS resolution without sacrificing sensitivity. More specifically, it would be desirable to maintain a given IMS resolution while simultaneously decreasing peak widths (i.e., overcoming diffusion). This would permit additional IMS separation to be performed and thus enable nearly unlimited resolution of isomeric species to be achieved. While such a method has yet to be developed, previous efforts have been made regarding the utility of spatial peak compression in IMS separations.[29−32] One such form of spatial peak compression, known as compression ratio ion mobility programming (CRIMP), is performed at the interface between two traveling wave (TW) regions.[29−31] In CRIMP, the first TW region operates in standard, separation, mode, while the second region intermittently moves (i.e., stutters). This enables multiple TW bins/troughs from the first region to be merged into a single, individual, TW bin/trough in the second region. For example, a compression ratio of 5 will merge 5 TW bins from the first region into 1 TW bin in the second region. In conjunction with in-SLIM ion accumulation on the order of seconds, a CRIMP step has demonstrated improved sensitivity as compared to ion introduction via an ion funnel trap.[30,33] Additionally, since long durations of in-SLIM ion accumulation will result in peak widths on the order of 10 s of milliseconds, CRIMP also enables a practical IMS separation to be performed on a large, starting, ion population.[29,30] Unfortunately, CRIMP has yet to show improved resolution for compounds with similar mobilities, especially when already starting with ion populations with narrow gate widths (e.g., narrow peak widths from ions introduced via an ion funnel). Furthermore, since ions are spatially compressed into the same TW bins, it is not surprising that IMS resolution will inherently decrease after a CRIMP step. Future work is needed to assess the full utility of CRIMP on complex mixtures. We note that currently CRIMP has only been performed in homebuilt SLIM IMS-based platforms, but nothing about its setup precludes being done in other TW-based devices.

While spatial compression of ions has been previously studied, as outlined above, temporal compression (i.e., in the time domain) has not been investigated in the context of traveling wave-based IMS-MS separations. Temporal compression (TC) can be performed by utilizing dynamic TW programming to increase the velocity of ions as they exit the IMS separation region. While the actual, physical, spacing of the ions remains unchanged (i.e., the spacing of the ions does change in spatial compression), the increased velocity of the ions effectively compresses them in the time domain (i.e., each IMS peak is compressed into fewer pushes to the time-of-flight mass spectrometer). A similar approach has recently been implemented on a DTIMS platform.[32] Herein, we present an investigation into the utility of temporal compression (TC) in a commercially available cIMS-MS platform.[12] Specifically, we were interested in assessing how TC affects the benchmarks of IMS separations (e.g., resolution and sensitivity). We hypothesized that TC would effectively increase the IMS signal intensity under the assumption that unwanted activation would not occur and thus reduce the overall peak area (i.e., a TC step would not significantly alter the overall IMS peak areas). Additionally, we also hypothesized that since ions are compressed temporally, rather than spatially, IMS resolution would be better preserved/maintained after a TC step is performed following an IMS separation (i.e., post-IMS).

EXPERIMENTAL SECTION

Reagents, Conditions, and cIMS Parameters

Reverse sequence peptide standards were purchased from Sigma-Aldrich (St. Louis, MO), D-monosaccharide standards (D-glucose, D-mannose, and D-galactose) were purchased from Carbosynth (Berkshire, U.K.), while L-monosaccharide standards (L-glucose, L-mannose, and L-galactose) were purchased from Sigma-Aldrich (St. Louis, MO). α-cyclodextrin was purchased from Tokyo Chemical Industry (Tokyo, Japan). Lactose was purchased from Carbosynth (Berkshire, U.K.), and lactose ($^{13}C_6$ Glc) was purchased from Santa Cruz Biotechnology (Dallas, TX). LC-MS grade solvents were purchased from Fisher Scientific (Pittsburgh, PA) and prepared at a final concentration of 49.75/49.75/0.5 (v/v) water/methanol/acetic acid. Reverse peptides were prepared at a concentration of 1 μM each. D/L-monosaccharides and α-cyclodextrin were prepared to a final concentration of 10 μM each. Lactose isotopologues were preprepared to a final concentration of 5 μM each.

The commercially available (Waters Corporation) cyclic ion mobility spectrometry-mass spectrometry (cIMS-MS) platform has been described extensively elsewhere.[12] Each sample was subjected to either positive (3 kV) or negative (2 kV) direct infusion electrospray ionization at flow rates of 2 μL/min (see figure captions for details). A quadrupole was used to mass filter selected m/z values or ranges of interest. The ∼1 m separation region was filled with N_2 to a pressure of 1.74 mbar, and a time-of-flight (TOF) MS operated in "V" mode was used for detection. The cIMS array allows for analyte-specific pathlengths by cycling ions multiple times around the separation region. Traveling wave conditions were optimized for each set of analytes (see figure captions and the Supporting Information for specific TW conditions used). MassLynx and Quartz were utilized to acquire and process the data, and Origin Pro 9.0 was used to determine peak areas and FWHM values. Each arrival time distribution was constructed by signal averaging for varying amounts of time (see figure captions and the Supporting Information) with no additional smoothing or post-processing performed.

https://doi.org/10.1021/acsmeasuresciau.2c00016
ACS Meas. Sci. Au 2022, 2, 361−369

Initial amplitude (V)	TC level	Final amplitude (V)
20	0	20
20	5	25
20	10	30

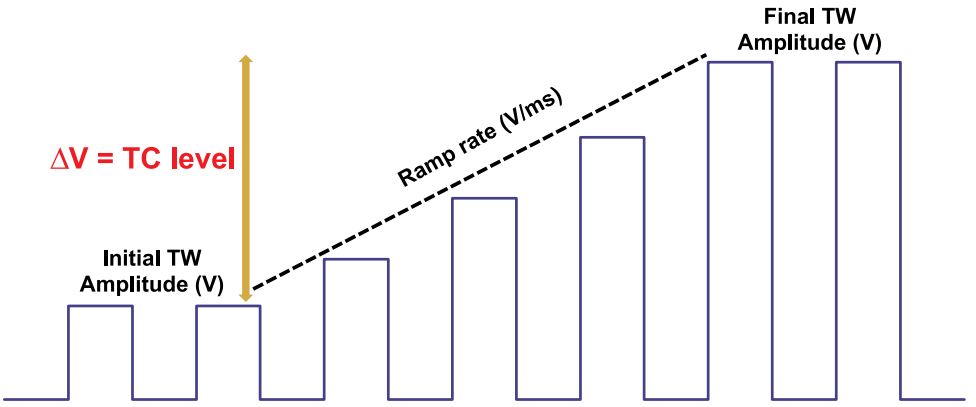

Figure 1. Schematic of temporal compression performed on a pulsed DC (square) traveling wave (TW). The temporal compression (TC) level is defined as the change in the TW amplitude (in volts, V) performed at a given ramp rate (4 V/ms was utilized in all experiments).

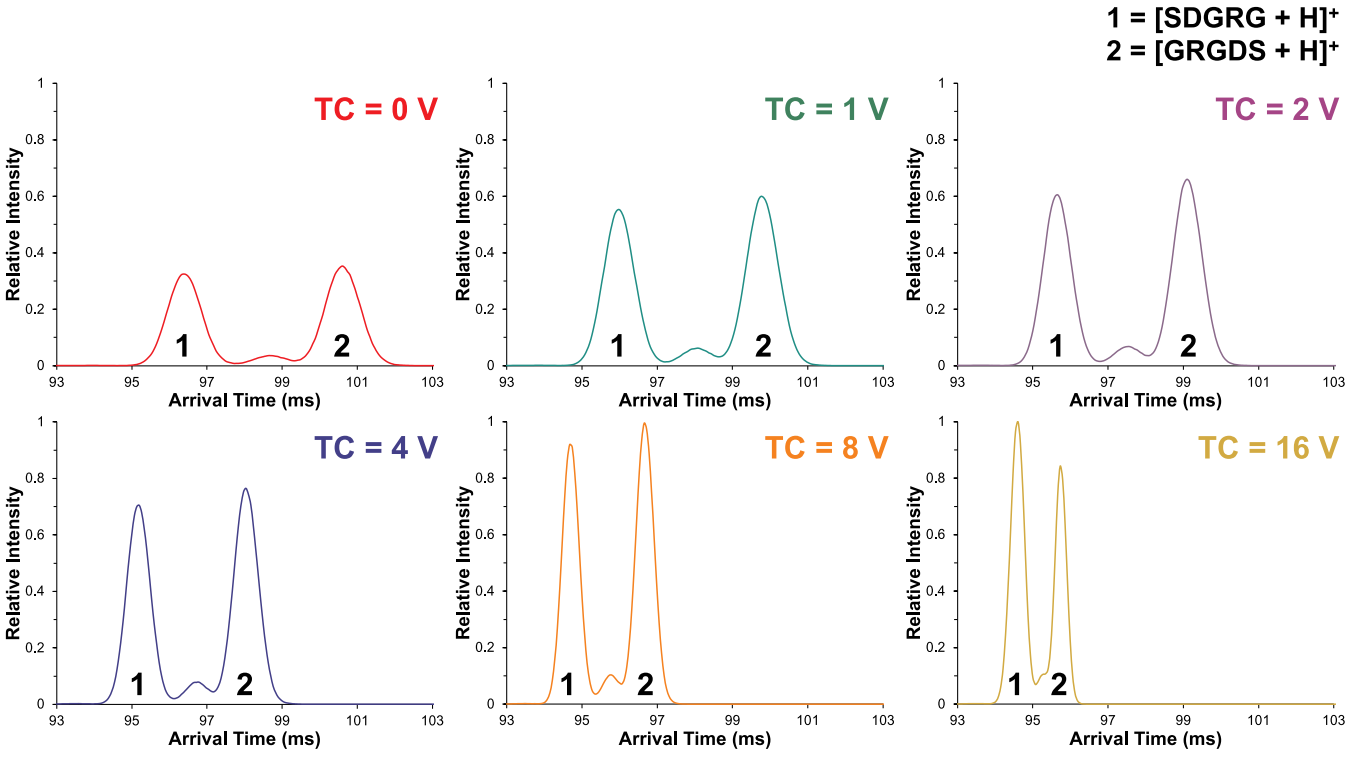

Figure 2. cIMS separation (10 m) of two reverse sequence peptide isomers as their $[M + H]^+$ species at traveling wave conditions of 400 m/s and 22 V. Varying levels of temporal compression were performed as described in Figure 1. Each cIMS separation was normalized to the highest intensity peak from all of the separations (TC level of 16 V). Signal averaging was performed for 2 min.

Temporal Compression

We are defining the temporal compression (TC) level as the net difference between the initial and final TW amplitudes of the cIMS array (Figure 1) during the ejection of ions to the TOF-MS. The cIMS separation region is orthogonal to the main track where ions enter as well as exit to the TOF for detection. Thus, during a cIMS separation, the array TW direction is sideways/orthogonal. Conversely, during the ejection of ions to the TOF, the array TW direction is forward. Temporal compression is performed by ramping the ejection TW amplitude in the software control (see the Supporting Information for an example screenshot of the software control and voltages used) and occurs exclusively in the 5 cm[12] long array region and not in the cIMS separation track or in the post-array. The mechanism for temporal compression results from increasing the TW amplitudes and thus causing the ions to have an increased velocity. At this increased velocity, fewer roll-over events would occur and thus the ions will be compressed temporally. We note that the highest possible TW that can be attained on this instrument is 50 V and the upper limit for a given ion would be when it would "surf" with the TW (i.e., have the same velocity as the TW). Data is only acquired during the final cIMS separation cycle and its duration is based on the m/z range surveyed. In all experiments, an m/z range up to 1200 was used and thus resulted in the eject/acquire step (see the Supporting

https://doi.org/10.1021/acsmeasuresciau.2c00016
ACS Meas. Sci. Au 2022, 2, 361−369

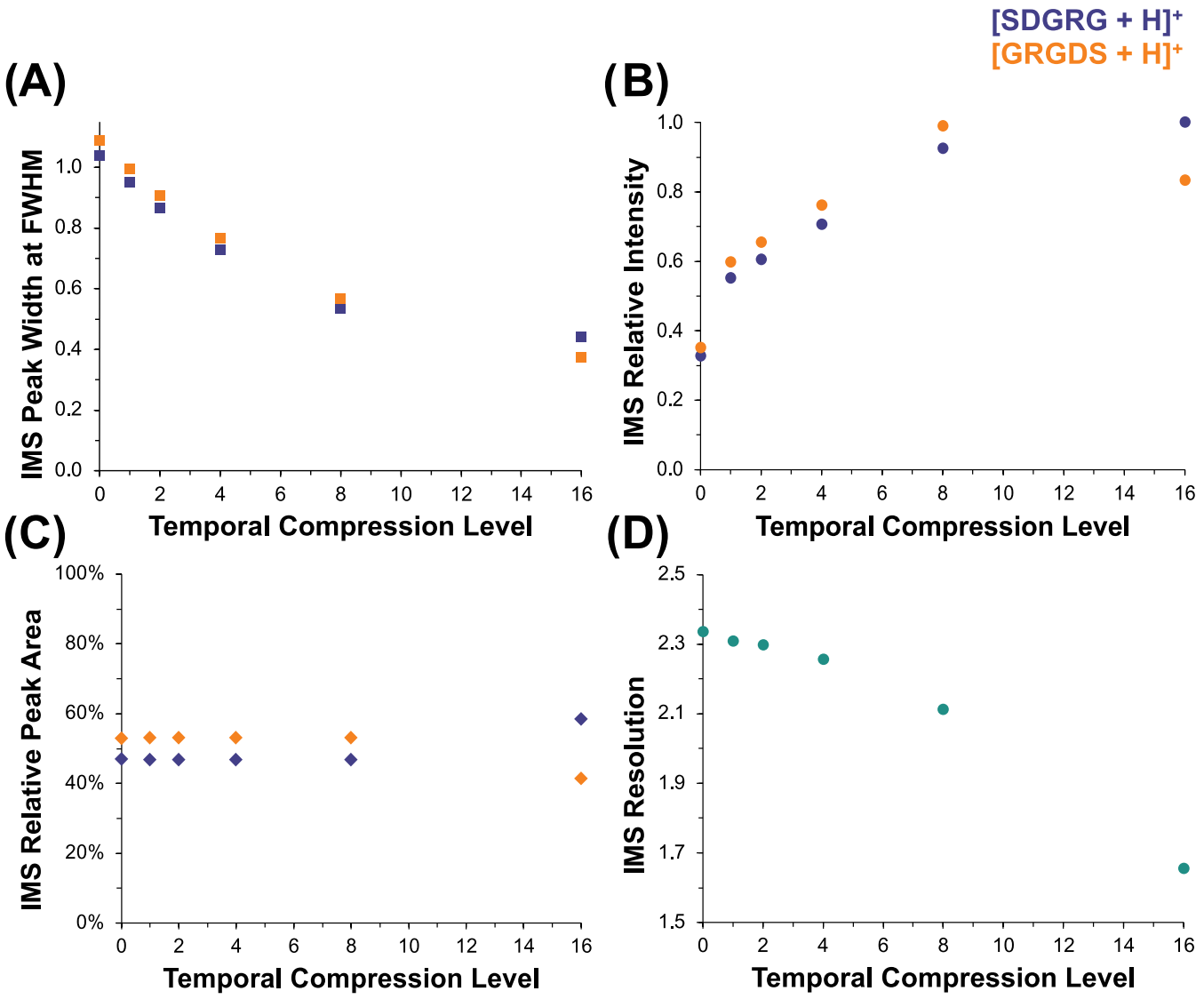

Figure 3. IMS metrics for [SDGRG + H]$^+$ (forward) and [GRGDS + H]$^+$ (reverse) peptides at varying TC levels at the same cIMS separation and TW conditions shown in Figure 2 for IMS peak widths (A), IMS relative peak intensities (B), IMS relative peak areas (C), and IMS resolution values (D).

Information) to be 13.20 ms in length, which corresponds to 200 pushes to the TOF (i.e., 0.066 ms per each push). This 13.20 ms includes both the separation time of the last cycle as well as the time required to scan up to m/z 1200 in the TOF. To ensure that the maximum amount of temporal compression was performed, we made sure that the temporal compression step began during the beginning of the final cycle (i.e., the first push/first 0.066 ms of the 13.20 ms ejection step on the final cycle). A discussion on the t_0 for a temporal compression step for the reverse sequence peptide isomers is in the Results and Discussion section. For further details of the instrument schematics as well as DC potentials used in a TC step, see the Supporting Information. A standard ramp rate of 4 V/ms was used in all experiments; we note that this ramp rate is the fastest permitted in the commercial software and enables all ions to be temporally compressed in the shortest amount of time permitted.

RESULTS AND DISCUSSION

Separation of Forward and Reverse Sequence Peptide Isomers

We first selected to assess the utility of temporal compression on the separation of two reverse sequence peptide isomers. These peptides were a logical starting point since they have been extensively studied in IMS and are a common standard used to characterize new IMS-MS platforms in terms of resolution, resolving power, sensitivity, ion losses, relative peak areas, etc.[12,34−39] We subjected these standard peptides to a 10 m cIMS-MS separation (Figure 2) with temporal compression (TC) levels ranging from 0 V (i.e., no TC; normal operation) to 16 V. Arrival time distributions in Figure 2 are normalized to the highest signal intensities observed across all TC levels. Our 10 m cIMS-MS separations of these reverse sequence peptide isomers with no TC applied (i.e., 0 V) match those previously reported in literature with other high-resolution IMS-MS platforms (i.e., both cIMS and SLIM IMS). Specifically, we observed a similar resolution of the isomers as previously reported as well as the presence of the additional conformation/substructure between the two main IMS peaks.

In examining our presented cIMS separations shown in Figure 2, we compared the IMS peak widths at FWHM, peak-to-peak resolution (eq 1), relative peak areas, and relative peak intensities across the varying TC levels applied (Figure 3).

https://doi.org/10.1021/acsmeasuresciau.2c00016
ACS Meas. Sci. Au 2022, 2, 361−369

From Figure 2 and the data shown in Figure 3, it is evident that as the TC level was increased to 8 V, peak widths at FWHM decreased by a factor of 2, while the resolution values only decreased by ∼5 to 10%, as compared to when no TC was applied. From our perspective, this indicates that care should be taken when describing traveling wave-based IMS separations in terms of resolving power rather than resolution given that our observed peak widths at a TC level of 8 V would imply an IMS resolving power twice as high as that of a TC level of 0 V. Additionally, we note that the relative peak areas for these peptides stayed constant from TC levels of 0 to 8 V, indicating that no unwanted fragmentation or activation occurred. However, at a TC level of 16 V, it appears that more considerable ion losses occur as shown by the diminished IMS resolution values as well as deviations in relative peak areas as compared to the other TC levels assessed. Thus, higher TC levels were not assessed since they would most likely result in unwanted fragmentation/activation and even more considerable signal loss than what was observed at a TC level of 16 V. Overall, our initial experiments exploring TC on the separation of these reverse sequence peptide isomers indicate that levels up to 8 V improved the overall separation in terms of increased IMS peak intensities as well as decreased peak widths at FWHM while maintaining similar IMS resolution and relative peak areas as compared to when no TC was applied (i.e., 0 V).

As was mentioned in the Experimental Section, TC is performed in the 5 cm cIMS array on the final cycle. To maximize the amount of time that ions undergo TC, we made sure that the temporal compression step began (i.e., t_0) during the beginning of the eject and acquire step (i.e., the first push/first 0.066 ms of the 13.20 ms ejection step on the final cycle). We note that this 13.20 ms includes both the separation time of the last cycle as well as the time required to scan up to m/z 1200 in the TOF. Specifically, for the reverse sequence peptide isomers, the t_0 for TC was ∼90.9 ms. Based on the arrival time of peak 1, we can calculate its velocity to be ∼104 m/s and thus would traverse the 5 cm array in ∼0.48 ms. If we assume an additional dead time of a few milliseconds, from contributions of ions traveling through the post-array region, transfer cell, and TOF, we can estimate that peak 1 is arriving at the array at a time point of ∼92 to 93 ms. Thus, with a TC ramp rate of 4 V/ms, the front of peak 1 will only experience a TC level of ∼8 to 10 V, while the tail of peak 1 and the entirety of peak 2 would fully experience a TC level of 16 V. Since peak 2 is undergoing this higher TC level for a longer duration, we believe this explains why it appears that peak 1 undergoes less TC than peak 2. This is evident by its time shift relative to a TC level of 0 V (e.g., at a TC level of 16 V, peak 1 shifts by ∼2 ms to the left, while peak 2 shifts by ∼3 ms to the left). Based on these above calculations, we have determined that the 2nd peak undergoes TC for a longer time period at 16 V than the first peak. As a result, we do indeed observe some peptide bond fragmentation as evidenced by the loss of serine corresponding to m/z 404 (see the Supporting Information).

Chiral Noncovalent Complexes: Separation of D/L Monosaccharides

While improvements were seen in peak intensities without compromising resolution when temporal compression was applied following the cIMS separation of the reverse sequence peptide isomers, we were also interested in assessing the utility of a TC step on the separation of potentially more fragile, noncovalent, complexes. Specifically, we were interested in developing a method to rapidly separate out various D/L monosaccharide enantiomer pairs with cIMS-MS and then subject each formed complex to a post-cIMS temporal compression step. As has been well stated in previous literature, enantiomeric separations remain one of the most challenging problems in the IMS-MS community.[40−45] Most previously developed methods for resolving enantiomers with IMS-MS have revolved around the formation of chiral, noncovalent, complexes and rely on not only the suitable formation of the initial complex but also that the formed diastereomeric complexes will be different enough in their structure to be separated.[43−45]

For this study, we chose the D/L pairs for glucose, galactose, and mannose. While the D-enantiomers are more common, the L-forms can also be present in an unknown biological sample.[46−48] We chose α-cyclodextrin (αCD) as the complexing molecule since previous work has shown for it to be effective in the enantiomeric separation of other small molecules, but it was unclear whether this would hold up for these highly polar monosaccharides (see Figure 4 for the structures of the monosaccharides and αCD).[43−45] Furthermore, rather than rely on metal adduction, which introduces ambiguity as to the actual metal concentration and thus precludes lab-to-lab reproducibility, we chose to analyze these complexes in negative ion mode as their deprotonated adducts. Each D/L pair was subjected to direct infusion both as an equimolar mixture as well as individually (see the Supporting Information for individual traces). In each case, the most abundant complex between the monosaccharides and αCD was $[M + 2\alpha CD - 2H]^{2-}$, which is unsurprising given that a similar 2:1 host−guest ratio was also observed in the cyclodextrin-based separations of D/L amino acids with SLIM IMS-MS.[43]

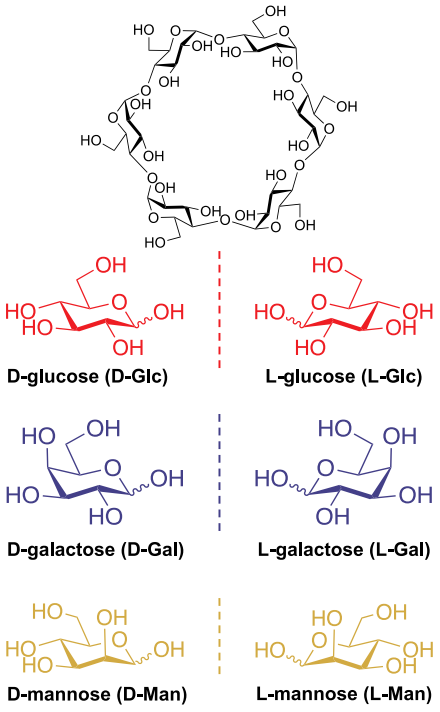

Figure 4. Structures for the D/L monosaccharide enantiomers and α-cyclodextrin.

https://doi.org/10.1021/acsmeasuresciau.2c00016
ACS Meas. Sci. Au 2022, 2, 361−369

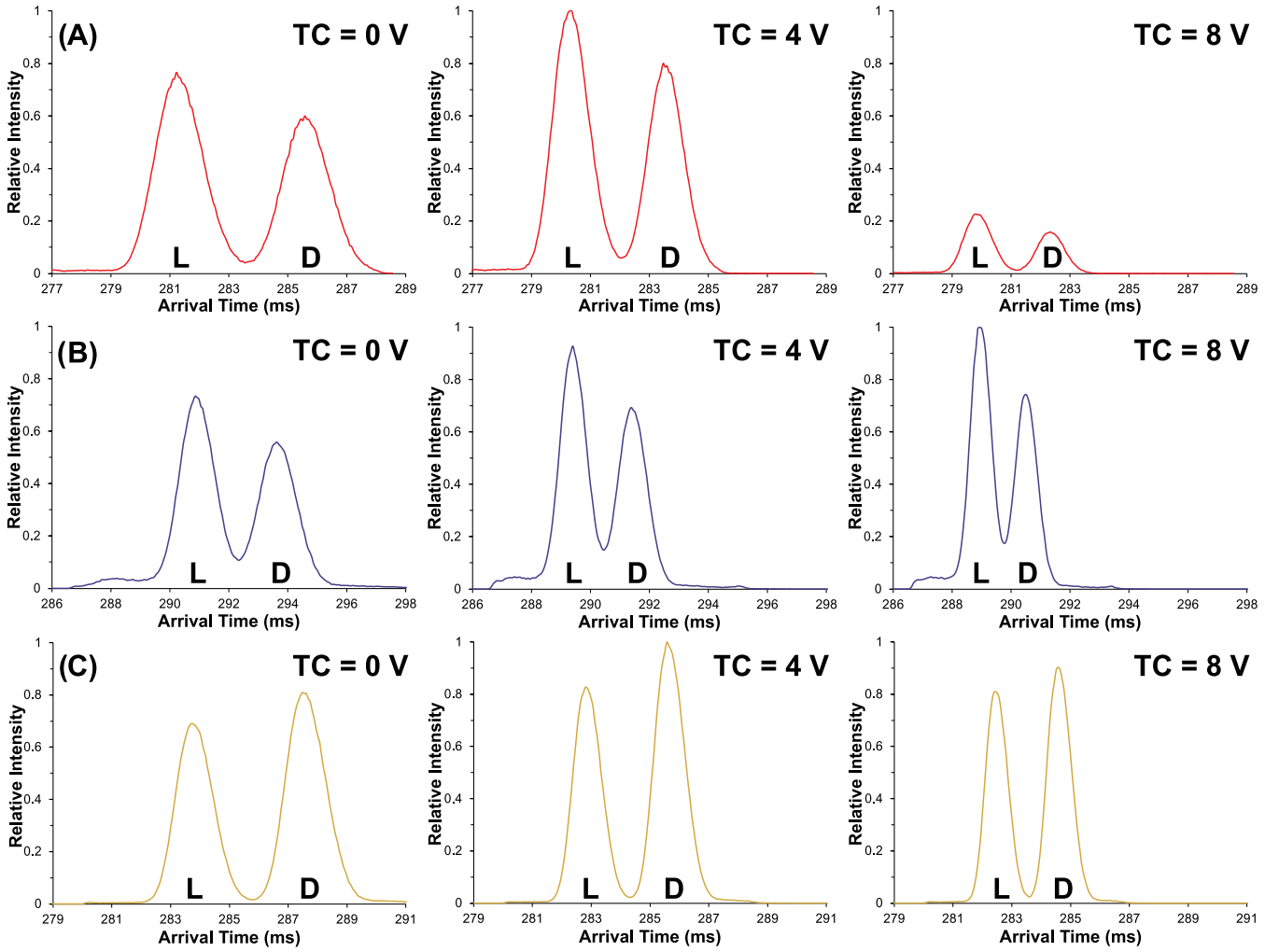

Figure 5. cIMS separation (25 m) of the D/L monosaccharides as their $[M + 2\alpha CD - 2H]^{2-}$ adducts at varying TC levels under TW conditions of 550 m/s and 27 V. Glucose (A; red), galactose (B; blue), and mannose (C; yellow). Signal averaging was performed for 2 min.

Each $[M + 2\alpha CD - 2H]^{2-}$ complex was subjected to 25 m of cIMS separation (Figure 5) under the same varying TC levels as were applied for the reverse sequence peptide isomers (i.e., 0–8 V; 16 V was not applied due to the activation observed for the peptides). Once again, each arrival time distribution shown in Figure 5 was normalized to the highest intensity observed across all TC levels assessed for each pair of monosaccharide enantiomers. It is noteworthy to mention that we observed enantiomeric separation in all cases after 25 m of cIMS separation, with the L-enantiomer always being higher mobility (i.e., arriving earlier) than its D-enantiomer counterpart, potentially indicating a diagnostic trend that needs to be assessed with other monosaccharides. For the individual traces of the D and L-enantiomers used to assign each peak in the enantiomeric mixtures in Figure 5, see the Supporting Information. At a TC level of 4 V, each peak in their respective cIMS separations increased in intensity by ∼20 to 30% with only an ∼4% decrease in peak-to-peak resolution (see the Supporting Information for resolution values for each separation as well as relative peak areas). However, when a TC level of 8 V was applied, a more significant decrease in peak intensities and relative peak areas was observed. This was indicated by fragmentation of the noncovalent complex, as shown in each respective mass spectrum (see the Supporting Information). We do note that while the peak intensities decreased at a TC level of 8 V, the resolution values between the D/L enantiomers stayed consistent with the other TC levels applied (i.e., 0 and 4 V). Nonetheless, from an analytical perspective, we have not only developed a rapid method to separate out the D/L enantiomers of glucose, galactose, and mannose but also have shown that a post-cIMS temporal compression step has broad utility for various molecules (i.e., peptides as well as noncovalent complexes). We note that the absolute value for the TC level applied can vary depending on the compounds of interest (e.g., 4 V for more labile species and 8 V for more rigid ones), thus optimization will most likely be necessary for the given analytes of interest.

Assessing Improvement in Peak Quality for Lactose Isotopologues

While our initial results indicate that a post-cIMS temporal compression has utility in increasing peak intensities and decreasing peak widths while maintaining peak-to-peak resolution and relative peak area values, we were also interested in assessing how temporal compression may improve peak quality. Specifically, at ultralong pathlength separations, it is expected that an IMS peak will be fairly broad in nature as a result of diffusion thus potentially precluding the ability to accurately identify its apex and peak width, which are important metrics in post-processing feature finding soft-

https://doi.org/10.1021/acsmeasuresciau.2c00016
ACS Meas. Sci. Au 2022, 2, 361–369

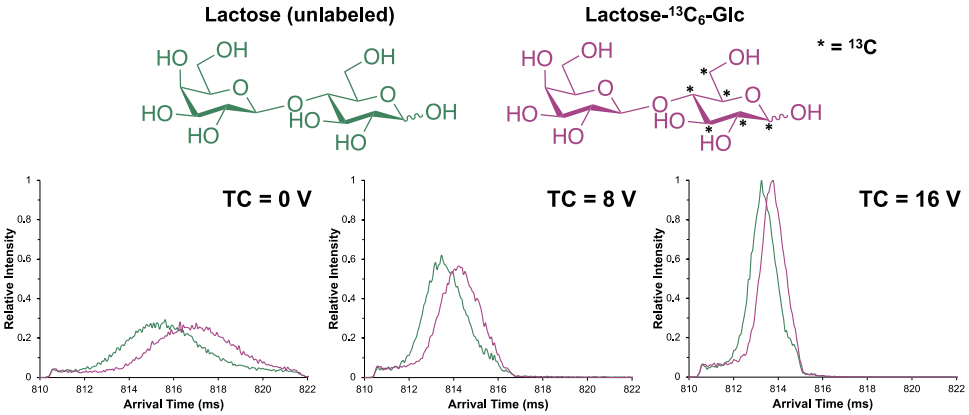

Figure 6. cIMS separation (65 m) of two lactose isotopologues at varying TC levels under TW conditions of 600 m/s and 22 V. The wraparound effect (i.e., where the fastest ions lap the slowest ones) can be observed for each arrival time distribution as the early-arriving elevated baseline. Signal averaging was performed for 30 s.

ware.[49−52] Our hypothesis was that a temporal compression step following an ultralong pathlength cIMS separation would enable improved peak quality and thus provide a better-defined peak shape for feature finding and/or peak picking algorithms.

Figure 6 shows the 65 m cIMS separation of two lactose isotopologues (i.e., $^{13}C_0$ and $^{13}C_6$-Glc) under varying levels of post-cIMS temporal compression. We note that no unwanted fragmentation or loss of peak area was observed at TC levels of 8 or 16 V, thus these were the conditions selected for these experiments; higher TC levels were not attempted because the software control does not permit TW amplitudes greater than 50 V. In comparing the cIMS separations for these lactose isotopologues (Figure 6), we observed that the IMS peak intensity at a TC level of 16 V was a factor of 4 greater as compared to when no TC was applied (i.e., 0 V). As a result, a less noisy IMS peak shape is observed at these higher TC levels for both lactose isotopologues thus demonstrating the improvement in peak quality when a post-cIMS temporal compression step is performed after ultralong pathlength separations. If we consider the unwanted higher mobility feature present at ∼810.5 ms (i.e., from the wraparound effect) as chemical noise in the IMS dimension, we observe a signal-to-noise (S/N) improvement of ∼3-fold when comparing the arrival time distributions at TC levels of 16 V versus 0 V. Future work is clearly needed to determine if such a temporal compression-based improvement in peak shapes will hold up in LC-IMS-MS-based workflows and thus enable higher-quality feature finding in post-processing search algorithms.

CONCLUSIONS

Herein, we have presented an assessment of the utility of a post-IMS temporal compression (TC) step in various high-resolution cIMS-MS separations that included reverse sequence peptide isomers, monosaccharide enantioseparations as their α-cyclodextrin-based noncovalent complexes, and lactose isotopologues. Specifically, we have demonstrated that temporal compression enables up to a four-fold increase in peak intensities and thus a four-fold decrease in FWHM peak widths without sacrificing peak-to-peak resolution or relative peak areas. Additionally, we observed improvement in peak quality as well as in S/N for the lactose isotopologues following a temporal compression step thus potentially benefiting peak identification in automated workflows. Our presented separations for the D/L monosaccharides as their α-cyclodextrin-based noncovalent complexes can be readily adapted into existing LC-IMS-MS workflows in a post-column addition fashion for rapid enantiomer identification. While, at this time, temporal compression remains limited to traveling wave-based IMS separations, we do note that temporal compression can easily be implemented on any commercial TWIMS-MS (e.g., MOBIE or cIMS) and homebuilt SLIM IMS-MS devices. We did not observe that a given TC level was optimal for each of the analyte sets studied, clearly indicating that TC conditions must be optimized for each individual molecule system of interest to maximize gains in peak intensity without any unwanted ion activation. We also note that no deviations in peak shapes were observed following TC; future work is clearly needed to assess the effect of a TC step on larger, and more conformationally flexible, molecules. Additionally, to the best of our knowledge, frequency-modulated TC is not currently available on commercial TWIMS platforms. Overall, we anticipate that TC-based strategies will be an added tool in the separation toolbox to help benefit the IMS-MS community.

ASSOCIATED CONTENT

Supporting Information

The Supporting Information is available free of charge at https://pubs.acs.org/doi/10.1021/acsmeasuresciau.2c00016.

Tables for the resolution and peak areas for each compound run; individual traces for the enantiomer separations; examples of a temporal compression time table (PDF)

AUTHOR INFORMATION

Corresponding Author

Gabe Nagy − *Department of Chemistry, University of Utah, Salt Lake City, Utah 84112, United States;* orcid.org/0000-0001-9007-4422; Email: gabe.nagy@utah.edu

Author

David L. Williamson − *Department of Chemistry, University of Utah, Salt Lake City, Utah 84112, United States;* orcid.org/0000-0002-8006-5933

Complete contact information is available at: https://pubs.acs.org/10.1021/acsmeasuresciau.2c00016

Notes

The authors declare no competing financial interest.

■ ACKNOWLEDGMENTS

The authors would like to thank the University of Utah for startup funds.

■ REFERENCES

(1) Gabelica, V.; Marklund, E. Fundamentals of ion mobility spectrometry. *Curr. Opin. Chem. Biol.* **2018**, *42*, 51−59.
(2) Dodds, J. N.; Baker, E. S. Ion Mobility Spectrometry: Fundamental Concepts, Instrumentation, Applications, and the Road Ahead. *J. Am. Soc. Mass Spectrom.* **2019**, *30*, 2185−2195.
(3) Shvartsburg, A. A.; Smith, R. D. Fundamentals of traveling wave ion mobility spectrometry. *Anal. Chem.* **2008**, *80*, 9689−9699.
(4) Burnum-Johnson, K. E.; Zheng, X.; Dodds, J. N.; Ash, J.; Fourches, D.; Nicora, C. D.; Wendler, J. P.; Metz, T. O.; Waters, K. M.; Jansson, J. K.; Smith, R. D.; Baker, E. S. Ion mobility spectrometry and the omics: Distinguishing isomers, molecular classes and contaminant ions in complex samples. *TrAC, Trends Anal. Chem.* **2019**, *116*, 292−299.
(5) Gabryelski, W.; Froese, K. L. Rapid and sensitive differentiation of anomers, linkage, and position isomers of disaccharides using High-Field Asymmetric Waveform Ion Mobility Spectrometry (FAIMS). *J. Am. Soc. Mass Spectrom.* **2003**, *14*, 265−277.
(6) Pathak, P.; Baird, M. A.; Shvartsburg, A. A. Identification of Isomers by Multidimensional Isotopic Shifts in High-Field Ion Mobility Spectra. *Anal. Chem.* **2018**, *90*, 9410−9417.
(7) Wu, Q.; Wang, J.-Y.; Han, D.-Q.; Yao, Z.-P. Recent advances in differentiation of isomers by ion mobility mass spectrometry. *TrAC, Trends Anal. Chem.* **2020**, *124*, No. 115801.
(8) Fernandez-Lima, F.; Kaplan, D. A.; Suetering, J.; Park, M. A. Gas-phase separation using a trapped ion mobility spectrometer. *Int. J. Ion Mobil. Spectrom.* **2011**, *14*, 93−98.
(9) Odenkirk, M. T.; Baker, E. S. Utilizing Drift Tube Ion Mobility Spectrometry for the Evaluation of Metabolites and Xenobiotics. In *Ion Mobility-Mass Spectrometry*, Springer, 2020; pp 35−54.
(10) Shvartsburg, A. A. *Differential Ion Mobility Spectrometry: Nonlinear Ion Transport and Fundamentals of FAIMS*, CRC Press, 2008.
(11) Deng, L.; Ibrahim, Y. M.; Baker, E. S.; Aly, N. A.; Hamid, A. M.; Zhang, X.; Zheng, X.; Garimella, S. V. B.; Webb, I. K.; Prost, S. A.; Sandoval, J. A.; Norheim, R. V.; Anderson, G. A.; Tolmachev, A. V.; Smith, R. D. Ion Mobility Separations of Isomers based upon Long Path Length Structures for Lossless Ion Manipulations Combined with Mass Spectrometry. *ChemistrySelect* **2016**, *1*, 2396−2399.
(12) Giles, K.; Ujma, J.; Wildgoose, J.; Pringle, S.; Richardson, K.; Langridge, D.; Green, M. A Cyclic Ion Mobility-Mass Spectrometry System. *Anal. Chem.* **2019**, *91*, 8564−8573.
(13) Deng, L.; Webb, I. K.; Garimella, S. V.; Hamid, A. M.; Zheng, X.; Norheim, R. V.; Prost, S. A.; Anderson, G. A.; Sandoval, J. A.; Baker, E. S.; et al. Serpentine ultralong path with extended routing (SUPER) high resolution traveling wave ion mobility-MS using structures for lossless ion manipulations. *Anal. Chem.* **2017**, *89*, 4628−4634.
(14) Harrilal, C. P.; Gandhi, V. D.; Nagy, G.; Chen, X.; Buchanan, M. G.; Wojcik, R.; Conant, C. R.; Donor, M. T.; Ibrahim, Y. M.; Garimella, S. V. B.; Smith, R. D.; Larriba-Andaluz, C. Measurement and Theory of Gas-Phase Ion Mobility Shifts Resulting from Isotopomer Mass Distribution Changes. *Anal. Chem.* **2021**, *93*, 14966−14975.
(15) Wojcik, R.; Nagy, G.; Attah, I. K.; Webb, I. K.; Garimella, S. V. B.; Weitz, K. K.; Hollerbach, A.; Monroe, M. E.; Ligare, M. R.; Nielson, F. F.; Norheim, R. V.; Renslow, R. S.; Metz, T. O.; Ibrahim, Y. M.; Smith, R. D. SLIM Ultrahigh Resolution Ion Mobility Spectrometry Separations of Isotopologues and Isotopomers Reveal Mobility Shifts due to Mass Distribution Changes. *Anal. Chem.* **2019**, *91*, 11952−11962.
(16) Wojcik, R.; Webb, I. K.; Deng, L.; Garimella, S. V.; Prost, S. A.; Ibrahim, Y. M.; Baker, E. S.; Smith, R. D. Lipid and glycolipid isomer analyses using ultra-high resolution ion mobility spectrometry separations. *Int. J. Mol. Sci.* **2017**, *18*, 183.
(17) Nagy, G.; Kedia, K.; Attah, I. K.; Garimella, S. V.; Ibrahim, Y. M.; Petyuk, V. A.; Smith, R. D. Separation of β-amyloid tryptic peptide species with isomerized and racemized l-aspartic residues with ion mobility in structures for lossless ion manipulations. *Anal. Chem.* **2019**, *91*, 4374−4380.
(18) Williamson, D. L.; Bergman, A. E.; Nagy, G. Investigating the Structure of α/β Carbohydrate Linkage Isomers as a Function of Group I Metal Adduction and Degree of Polymerization as Revealed by Cyclic Ion Mobility Separations. *J. Am. Soc. Mass Spectrom.* **2021**, *32*, 2573−2582.
(19) Williamson, D. L.; Bergman, A. E.; Heider, E. C.; Nagy, G. Experimental Measurements of Relative Mobility Shifts Resulting from Isotopic Substitutions with High-Resolution Cyclic Ion Mobility Separations. *Anal. Chem.* **2022**, *94*, 2988−2995.
(20) Garimella, V. B. S.; Nagy, G.; Ibrahim, Y. M.; Smith, R. D. Opening new paths for biological applications of ion mobility - Mass spectrometry using structures for lossless ion manipulations. *TrAC, Trends Anal. Chem.* **2019**, *116*, 300−307.
(21) Gabelica, V.; Shvartsburg, A. A.; Afonso, C.; Barran, P.; Benesch, J. L.; Bleiholder, C.; Bowers, M. T.; Bilbao, A.; Bush, M. F.; Campbell, J. L.; et al. Recommendations for reporting ion mobility Mass Spectrometry measurements. *Mass Spectrom. Rev.* **2019**, *38*, 291−320.
(22) Rokushika, S.; Hatano, H.; Baim, M. A.; Hill, H. H. Resolution measurement for ion mobility spectrometry. *Anal. Chem.* **1985**, *57*, 1902−1907.
(23) Asbury, G. R.; Hill, H. H., Jr Evaluation of ultrahigh resolution ion mobility spectrometry as an analytical separation device in chromatographic terms. *J. Microcolumn Sep.* **2000**, *12*, 172−178.
(24) Grabarics, M.; Lettow, M.; Kirk, A. T.; von Helden, G.; Causon, T. J.; Pagel, K. Plate-height model of ion mobility-mass spectrometry. *Analyst* **2020**, *145*, 6313−6333.
(25) Grabarics, M.; Lettow, M.; Kirk, A. T.; von Helden, G.; Causon, T. J.; Pagel, K. Plate-height model of ion mobility-mass spectrometry: Part 2—Peak-to-peak resolution and peak capacity. *J. Sep. Sci.* **2021**, *44*, 2798−2813.
(26) Ben Faleh, A.; Warnke, S.; Rizzo, T. R. Combining Ultrahigh-Resolution Ion-Mobility Spectrometry with Cryogenic Infrared Spectroscopy for the Analysis of Glycan Mixtures. *Anal. Chem.* **2019**, *91*, 4876−4882.
(27) Deng, L.; Ibrahim, Y. M.; Hamid, A. M.; Garimella, S. V. B.; Webb, I. K.; Zheng, X.; Prost, S. A.; Sandoval, J. A.; Norheim, R. V.; Anderson, G. A.; Tolmachev, A. V.; Baker, E. S.; Smith, R. D. Ultra-High Resolution Ion Mobility Separations Utilizing Traveling Waves in a 13 m Serpentine Path Length Structures for Lossless Ion Manipulations Module. *Anal. Chem.* **2016**, *88*, 8957−8964.
(28) Peterson, T. L.; Nagy, G. Toward Sequencing the Human Milk Glycome: High-Resolution Cyclic Ion Mobility Separations of Core Human Milk Oligosaccharide Building Blocks. *Anal. Chem.* **2021**, *93*, 9397−9407.
(29) Garimella, S. V. B.; Hamid, A. M.; Deng, L.; Ibrahim, Y. M.; Webb, I. K.; Baker, E. S.; Prost, S. A.; Norheim, R. V.; Anderson, G. A.; Smith, R. D. Squeezing of ion populations and peaks in traveling wave ion mobility separations and structures for lossless ion manipulations using compression ratio ion mobility programming. *Anal. Chem.* **2016**, *88*, 11877−11885.
(30) Deng, L.; Garimella, S. V.; Hamid, A. M.; Webb, I. K.; Attah, I. K.; Norheim, R. V.; Prost, S. A.; Zheng, X.; Sandoval, J. A.; Baker, E. S.; et al. Compression ratio ion mobility programming (CRIMP) accumulation and compression of billions of ions for ion mobility-mass spectrometry using traveling waves in structures for lossless ion manipulations (SLIM). *Anal. Chem.* **2017**, *89*, 6432−6439.
(31) Garimella, S. V. B.; Ibrahim, Y. M.; Tang, K.; Webb, I. K.; Baker, E. S.; Tolmachev, A. V.; Chen, T.-C.; Anderson, G. A.; Smith,

https://doi.org/10.1021/acsmeasuresciau.2c00016
ACS Meas. Sci. Au 2022, 2, 361−369

R. D. Spatial ion peak compression and its utility in ion mobility spectrometry. *J. Am. Soc. Mass Spectrom.* **2016**, *27*, 1128−1135.
(32) Chen, X.; Latif, M.; Gandhi, V. D.; Chen, X.; Hua, L.; Fukushima, N.; Larriba-Andaluz, C. Enhancing Separation and Constriction of Ion Mobility Distributions in Drift Tubes at Atmospheric Pressure Using Varying Fields. *Anal. Chem.* **2022**, *94*, 5690−5698.
(33) Chouinard, C. D.; Nagy, G.; Webb, I. K.; Garimella, S. V. B.; Baker, E. S.; Ibrahim, Y. M.; Smith, R. D. Rapid Ion Mobility Separations of Bile Acid Isomers Using Cyclodextrin Adducts and Structures for Lossless Ion Manipulations. *Anal. Chem.* **2018**, *90*, 11086−11091.
(34) Giles, K.; Williams, J. P.; Campuzano, I. Enhancements in travelling wave ion mobility resolution. *Rapid Commun. Mass Spectrom.* **2011**, *25*, 1559−1566.
(35) Wu, C.; Siems, W. F.; Klasmeier, J.; Hill, H. H. Separation of isomeric peptides using electrospray ionization/high-resolution ion mobility spectrometry. *Anal. Chem.* **2000**, *72*, 391−395.
(36) Hollerbach, A. L.; Li, A.; Prabhakaran, A.; Nagy, G.; Harrilal, C. P.; Conant, C. R.; Norheim, R. V.; Schimelfenig, C. E.; Anderson, G. A.; Garimella, S. V. B.; Smith, R. D.; Ibrahim, Y. M. Ultra-High-Resolution Ion Mobility Separations Over Extended Path Lengths and Mobility Ranges Achieved using a Multilevel Structures for Lossless Ion Manipulations Module. *Anal. Chem.* **2020**, *92*, 7972−7979.
(37) Deng, L.; Ibrahim, Y. M.; Baker, E. S.; Aly, N. A.; Hamid, A. M.; Zhang, X.; Zheng, X.; Garimella, S. V.; Webb, I. K.; Prost, S. A.; et al. Ion mobility separations of isomers based upon long path length structures for lossless ion manipulations combined with mass spectrometry. *ChemistrySelect* **2016**, *1*, 2396−2399.
(38) Enders, J. R.; Mclean, J. A. Chiral and structural analysis of biomolecules using mass spectrometry and ion mobility-mass spectrometry. *Chirality* **2009**, *21*, E253−E264.
(39) Keelor, J. D.; Zambrzycki, S.; Li, A.; Clowers, B. H.; Fernández, F. M. Atmospheric pressure drift tube ion mobility−Orbitrap mass spectrometry: initial performance characterization. *Anal. Chem.* **2017**, *89*, 11301−11309.
(40) Dwivedi, P.; Wu, C.; Matz, L. M.; Clowers, B. H.; Siems, W. F.; Hill, H. H. Gas-phase chiral separations by ion mobility spectrometry. *Anal. Chem.* **2006**, *78*, 8200−8206.
(41) Mie, A.; Jörntén-Karlsson, M.; Axelsson, B.-O.; Ray, A.; Reimann, C. T. Enantiomer separation of amino acids by complexation with chiral reference compounds and high-field asymmetric waveform ion mobility spectrometry: Preliminary results and possible limitations. *Anal. Chem.* **2007**, *79*, 2850−2858.
(42) Pérez-Míguez, R.; Bruyneel, B.; Castro-Puyana, M.; Marina, M. L.; Somsen, G. W.; Domínguez-Vega, E. Chiral discrimination of DL-amino acids by trapped ion mobility spectrometry after derivatization with (+)-1-(9-fluorenyl) ethyl chloroformate. *Anal. Chem.* **2019**, *91*, 3277−3285.
(43) Nagy, G.; Chouinard, C. D.; Attah, I. K.; Webb, I. K.; Garimella, S. V.; Ibrahim, Y. M.; Baker, E. S.; Smith, R. D. Distinguishing enantiomeric amino acids with chiral cyclodextrin adducts and structures for lossless ion manipulations. *Electrophoresis* **2018**, *39*, 3148−3155.
(44) Yang, S.; Gu, L.; Wu, F.; Dai, X.; Xu, F.; Li, Q.; Fang, X.; Yu, S.; Ding, C.-F. The chirality determination of amino acids by forming complexes with cyclodextrins and metal ions using ion mobility spectrometry, and a DFT calculation. *Talanta* **2022**, *243*, No. 123363.
(45) Yang, S.; Wu, F.; Yu, F.; Gu, L.; Wang, H.; Liu, Y.; Chu, Y.; Wang, F.; Fang, X.; Ding, C.-F. Distinction of chiral penicillamine using metal-ion coupled cyclodextrin complex as chiral selector by trapped ion mobility-mass spectrometry and a structure investigation of the complexes. *Anal. Chim. Acta* **2021**, *1184*, No. 339017.
(46) Barron, L. D. Chirality and Life. In *Strategies of Life Detection*, Springer, 2008; pp 187−201.
(47) Hein, J. E.; Blackmond, D. G. On the origin of single chirality of amino acids and sugars in biogenesis. *Acc. Chem. Res.* **2012**, *45*, 2045−2054.
(48) Nagy, G.; Pohl, N. L. Complete hexose isomer identification with mass spectrometry. *J. Am. Soc. Mass Spectrom.* **2015**, *26*, 677−685.
(49) Szymańska, E.; Davies, A. N.; Buydens, L. M. Chemometrics for ion mobility spectrometry data: recent advances and future prospects. *Analyst* **2016**, *141*, 5689−5708.
(50) Sivalingam, G. N.; Yan, J.; Sahota, H.; Thalassinos, K. Amphitrite: A program for processing travelling wave ion mobility mass spectrometry data. *Int. J. Mass Spectrom.* **2013**, *345*−*347*, 54−62.
(51) Feuerstein, M. L.; Kurulugama, R. T.; Hann, S.; Causon, T. Novel acquisition strategies for metabolomics using drift tube ion mobility-quadrupole resolved all ions time-of-flight mass spectrometry (IM-QRAI-TOFMS). *Anal. Chim. Acta* **2021**, *1163*, No. 338508.
(52) Chouinard, C. D.; Nagy, G.; Webb, I. K.; Shi, T.; Baker, E. S.; Prost, S. A.; Liu, T.; Ibrahim, Y. M.; Smith, R. D. Improved Sensitivity and Separations for Phosphopeptides using Online Liquid Chromotography Coupled with Structures for Lossless Ion Manipulations Ion Mobility−Mass Spectrometry. *Anal. Chem.* **2018**, *90*, 10889−10896.

https://doi.org/10.1021/acsmeasuresciau.2c00016
ACS Meas. Sci. Au 2022, 2, 361−369